Optic cavitation in an ultrasonic field

Thomas Kurz,* Dennis Kröninger, Reinhard Geisler, and Werner Lauterborn
Drittes Physikalisches Institut, Universität Göttingen, Friedrich-Hund-Platz 1, D-37077 Göttingen, Germany
(Received 10 November 2005; revised manuscript received 13 October 2006; published 12 December 2006)

Cavitation bubbles are generated in water by low-energy femtosecond laser pulses in the presence of an ultrasonic field. Bubble dynamics and cavitation luminescence are investigated by CCD photography and photomultiplier measurements in dependence on the phase of the acoustic cycle at which the bubbles are generated. The experimental results demonstrate that the initially small laser-generated bubbles can be expanded significantly by the sound field and that weak cavitation luminescence can be observed in two small intervals of the seeding phase. The luminescence yield sensitively depends on the degree of sphericity of bubble collapse.

DOI: 10.1103/PhysRevE.74.066307 PACS number(s): 47.55.dp, 47.55.D−, 78.60.Mq, 43.35.+d

I. INTRODUCTION

In optic cavitation the light of a pulsed laser is focused in a liquid whereupon transient bubbles are produced by optical breakdown [1,2]. With this method bubbles can be placed in the liquid at precisely defined points in space and time for experimental investigation. The collapse dynamics and shock-wave emission of such bubbles have been studied in great detail at different conditions by means of, e.g., high-speed photography and holography [3]. In particular, it has been demonstrated that bubbles collapsing near a rigid wall are penetrated by a liquid jet. The ensuing toroidal collapse can be linked to erosion damage on the wall surface [4]. Laser-produced bubbles also feature cavitation luminescence when they collapse sufficiently spherical [5,6]. Its intensity and pulse length are related to the bubble size [5,7,8].

Because of their high breakdown threshold and long interaction time, laser pulses of nanosecond duration typically generate large bubbles (maximum radius $\gtrsim$0.5 mm). To obtain bubbles with smaller sizes, comparable to those encountered, e.g., in single-bubble sonoluminescence (SBSL) experiments [9], shorter laser pulses in the picosecond and femtosecond regions have to be used [10,11]. With femtosecond pulses, however, nonlinear optical effects (self-focusing, moving foci) lead to possibly long plasma channels and thus cylindrically shaped bubbles. These bubbles collapse by forming axial indentations [12], and no cavitation luminescence has been found for them [13].

In a quiet liquid energy is supplied to an optically generated bubble only initially when the laser pulse is absorbed and heats the medium. The hot spot expands explosively, giving off a part of its energy into a shock wave and converting a part into potential energy of the expanded bubble. Subsequently, the energy is quickly dissipated during collapse, rebound, and afterbounces with decaying amplitude. At this stage, the bubble usually suffers severe shape distortions, leading to its disruption and disintegration into microbubbles. The size and mechanical energy of the bubble rise with laser pulse energy. However, a practical limit exists for the generation of useful bubbles, because the plasma cone gets more elongated with rising laser energy and more gas and vapor are generated that fill the bubble. Both effects facilitate the onset of shape perturbations, leading to bubble instability. Furthermore, bubble collapse cannot be made more violent, to yield more extreme conditions in the bubble, by simply producing larger cavities as the medium within acts to cushion the collapse.

The present work addresses the question of how the collapse and luminescence of laser-induced bubbles can be upscaled. It is motivated by the idea that bubbles created with very short laser pulses, having a small breakdown energy and giving a small initial amount of gas and vapor should strongly expand under the influence of an intense ultrasonic field when they are created in the sonic tension phase. In this way, bubbles with rest radii of a few micrometers, comparable to those of SBSL bubbles, can be driven with acoustic pressures above the limit imposed by stable diffusive equilibrium in SBSL. The primary objective was to detect cavitation luminescence, as an indicator for strong excitation of the bubble medium, for bubbles created with a femtosecond laser at suitable phases of the driving sound field.

The transient response of a bubble to a single acoustical cycle has been considered theoretically (see [14] and references therein). For its experimental investigation, compared to pulsed ultrasonic excitation of bubble nuclei, laser seeding of bubbles in a stationary sound field has several advantages: (i) there are no pulse edges that could compromise acoustic driving of the bubble; (ii) high sound amplitudes can be achieved easily at an acoustic resonance of the container; (iii) the bubbles have well-defined and reproducible initial parameters; (iv) the sound field does not have to do work against the surface tension initially, and the energy deposited by the laser pulse can be utilized at proper choice of the seeding phase.

It has been shown previously that the luminescence of bubbles optically generated in a sound field depends on the phase at which the bubbles are seeded [15]. In this experiment, a Nd:YAG laser was used (8 ns pulse width) that produced large bubbles with collapse times above 100 μs. To drive these bubbles effectively a low-frequency sound field was required that could not be built up resonantly in the small cuvette used for the experiment. Thus, the sound field amplitude was comparatively low and the effect not very pronounced.

*Electronic address: Thomas.Kurz@physik.uni-goettingen.de

 ©2006 The American Physical Society

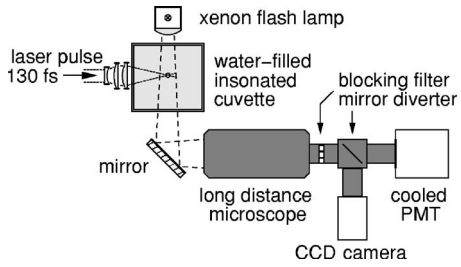

FIG. 1. Sketch of the experimental setup.

In this investigation bubbles in water are produced that are sufficiently small to be efficiently excited in a standing ultrasonic wave field with an amplitude just below the acoustic cavitation threshold. A significant increase of maximum bubble radii and collapse times is observed when choosing a suitable seeding phase. Weak cavitation luminescence can in fact be detected in two small phase intervals. It is supposed to occur because of enhanced collapse strength (compared to the nondriven bubble) and, equally important, because bubble collapse is sufficiently spherical for these seeding phases.

II. EXPERIMENT

A sketch of the experimental setup is shown in Fig. 1. Single laser pulses (duration 130 fs, wavelength 810 nm) having energies of less than 1 μJ (adjusted by a variable beam splitter) are obtained from an amplified Ti:sapphire laser system (Tsunami oscillator and Spitfire regenerative amplifier, Spectra Physics). Bubbles are generated in water at room temperature at a rate of about 0.5 Hz by focusing the laser pulses in a rectangular cuvette by means of an aberration-minimized triplet lens. As the laser energy may fluctuate the pulse energy is monitored by a photodiode. The cuvette (silica glass, 30 mm$\times$30 mm$\times$30 mm) is insonated by a piezotransducer, glued to its bottom, at the resonance frequency of the (1,1,1) mode, $f_a \approx 44.6$ kHz, which depends on the fill level. The sound field is switched off between the laser shots to minimize heating of the liquid by dissipated acoustic energy and also to prevent bubbles remaining from the previous shot from getting trapped near the pressure antinode. The resonance of the chamber is checked continually and the frequency is adjusted if necessary to keep the sound pressure at a constant level. Drift of the resonance frequency is caused primarily by changes in the ambient temperature and by water evaporation. To keep the effect on pressure amplitude small, the cuvette is mechanically damped to broaden the resonance. The gas content of the liquid does not play an important role in the dynamics of transient laser-generated bubbles [8,16] and has not been controlled in this experiment. It does, however, influence the acoustic cavitation threshold which sets a limit to the sound amplitude that can be applied.

As hydrophones tend to disturb the sound field (here, mainly by changing the resonance frequency) and the bubble collapse in the cuvette significantly, the acoustic pressure p_a is determined indirectly by numerically fitting a Gilmore model to the observed radial dynamics of the bubble with p_a as the free parameter. This method gives pressure amplitudes that are consistent with hydrophone measurements taken at the same transducer voltage, without bubbles.

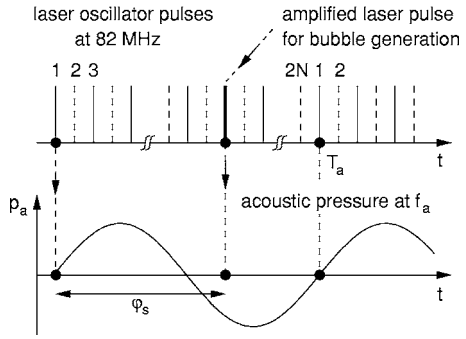

FIG. 2. Synchronization of the acoustic field with the laser oscillator by phase-locking circuitry. The bubbles can be generated at certain phases φ_s of the acoustic cycle by picking and amplifying the corresponding (odd-numbered) pulse of the laser oscillator.

The experiment employs a fast CCD camera (Imager 3, LaVision, pixel size 9.9 μm) for image acquisition and a sensitive, cooled photomultiplier (R3809U with thermoelectric cooler C4878, Hamamatsu) connected to a fast oscilloscope (Infinium 54845A, Agilent). The cooling of the photomultiplier reduces spurious counts to a negligible level. The detectors are mounted to a long-distance mirror microscope (QM 100, Questar) with Barlow lens, via a dielectric filter blocking the laser wavelength. A mirror diverter permits one to take images (xenon-flash lamp illumination, exposure time 200 ns) and photomultiplier measurements of cavitation luminescence in immediate succession so experimental parameters will remain approximately constant for the two measurements. Image magnification is 27-fold, giving an image scale of 0.37 μm/pixel.

Stable synchronization between the acoustic field and the laser oscillator is required to generate bubbles at an exactly defined phase φ_s of the acoustic cycle. For this reason the ultrasonic signal is derived from the laser oscillator frequency (f_L=82 MHz) by a custom-built divider and phase-locking electronics, giving acoustic frequencies $f_a = f_L/2N$, where N is an integer chosen that f_a matches the resonance frequency of the cuvette as closely as possible (Fig. 2). Furthermore, the device generates the necessary signals for stable operation of the pump laser and the timing signals for selecting, with adjustable delay, a single-seed laser pulse for amplification and bubble generation. It also features a trigger signal arriving with fixed time delay before the laser pulse. This signal is fed into a delay generator (DG 535, Stanford Research Systems), which, in turn, controls the timing of the flash lamp and CCD camera. The laser controller, delay generator, and oscilloscope are operated by a computer to allow automatic measurements, while image acquisition is performed with a second computer.

The dynamics of bubbles generated with laser pulses of about the same energy turns out to be well reproducible. Thus, as in many previous studies, it is investigated here by assembling frames taken with constant time separation (100 ns or 200 ns) into image series. Each series is analyzed by means of digital image processing (scaling, adjustment of

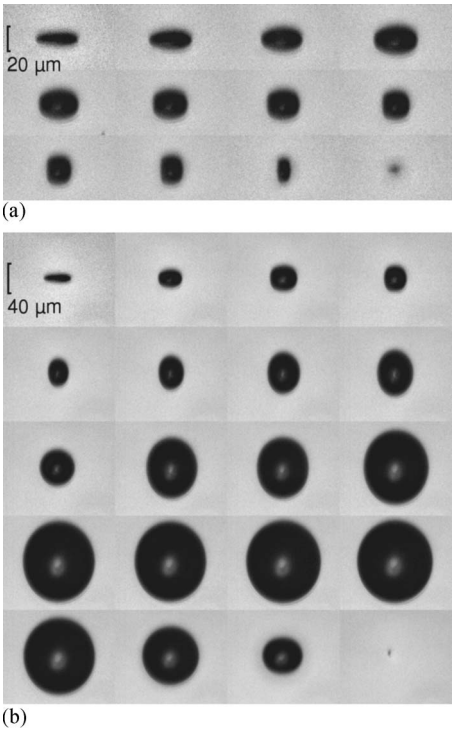

FIG. 3. (a) Dynamics of an elongated bubble produced by a 130-fs laser pulse of energy 0.22 μJ in water without a sound field. The frames are taken at 200-ns intervals. (b) Bubble generated by a laser pulse with the same parameters in a sound field of amplitude 159 kPa at seeding phase 192°. The frame separation is now 800 ns.

brightness and contrast, extraction of bubble parameters, and composition of streak images).

Figure 3(a) shows an example of a bubble generated in water with a laser pulse of 130 fs duration and of 0.22 μJ energy (this value is corrected for the transmission of the focusing optics). The elongated breakdown channel leads to an elliptical bubble of maximum size $\approx 30\ \mu\text{m} \times 55\ \mu\text{m}$ that collapses within 2.2 μs. During collapse, the bubble presumably develops two axial indentations, so the bubble shape and collapse dynamics are far from being spherical. Figure 3(b) exemplifies the dynamics of a bubble seeded in an ultrasonic field with the same laser energy and pulse duration (note the different frame separation and image scale). With a sound field of 159 kPa amplitude the bubble expands to about 100 μm diameter and assumes an approximately spherical shape. The ensuing collapse is also nearly spherical and takes place 15 μs after bubble generation. Of course, the dynamics depends on the phase of the sound field at which the bubble is generated. In the example shown, the bubble was shot in the tension phase of the sinusoidal acoustic cycle (at phase $\varphi_s = 192^\circ$). A rough estimate of energy gain by acoustic driving gives a nearly tenfold increase of collapse energy from ≈ 10 nJ of the nondriven bubble [Fig. 3(a)] to ≈ 100 nJ of the driven bubble [Fig. 3(b)].

III. NUMERICAL SIMULATIONS

The numerical simulations are based on the Gilmore model for spherical bubbles [17,18]. It is a first-order model

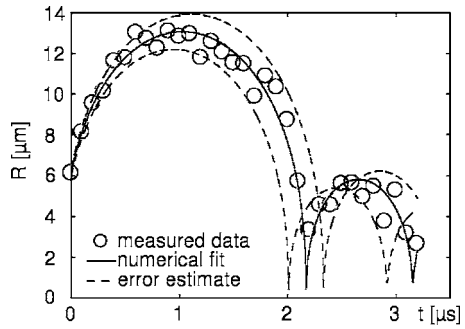

FIG. 4. Radius vs time of a bubble without acoustic excitation generated by a laser pulse of energy 0.22 μJ. Experimental data (circles) are obtained as averages over three laser shots. The solid line shows a numerical calculation with best-fit initial conditions. The dashed lines represent the radial dynamics at ±4.5% deviation of laser pulse energy.

in the Mach number that incorporates compressibillity effects, viscosity, and surface tension of the liquid. For the bubble interior, a van der Waals hard core law with a polytropic exponent of $\kappa = 4/3$ is assumed. The volume oscillations of weakly nonspherical, nearly ellipsoidal bubbles, as observed in our experiment, can be well approximated by a spherical bubble model. To compare experimental with simulated radial dynamics, the equivalent radius of a sphere is calculated from the bubble volume that is extracted from the recorded images by measuring the semiaxes of the ellipsoid along the direction of the laser beam and perpendicular to it.

The amplitude and phase of the sound field are determined indirectly by a numerical fit of the observed radial dynamics to solutions of the Gilmore model. For the simulation the initial data $R(0)$, $\dot{R}(0)$ and the equilibrium radius R_m must be known. The initial radius $R(0)$ is measured directly on the images with about 10% accuracy. The remaining initial parameters are obtained from bubbles that are not acoustically excited but created with the same laser pulse energy as the driven bubbles. Figure 4 shows the experimental radius-time curve for a laser energy of $E_L = 0.22$ μJ. Each data point corresponds to an average taken over three bubbles. The solutions of the numerical model are compared to the observed dynamics and $\dot{R}(0)$ and R_m are sought for that minimize the least-squares error of the fit. It is assumed that these quantities only depend on the shape and energy deposit of the laser plasma but not on the sound pressure amplitude. Neglecting mass flow by gas diffusion and vapor evaporation and condensation during the observation interval, the following bubble parameters have been found for a laser pulse energy of $E_L = 0.22$ μJ and used for further analysis: $R(0) = 6.2 \pm 0.9$ μm, $\dot{R}(0) = 26.2(+1.7, -1.8)$ m/s, and $R_m = 2.5 \pm 0.17$ μm.

The radial dynamics numerically calculated with these initial conditions is given in Fig. 4 by the solid line. Fluctuations of the laser pulse energy E_L are the main source of error in the bubble parameters. The error margins stated above correspond to the measured maximum deviations of laser energy, $\Delta E_L / E_L \approx \pm 4.5\%$. To estimate the error thereby introduced in the bubble dynamics, a linear regression for the

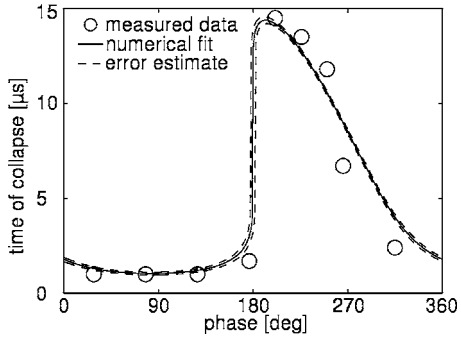

FIG. 5. Collapse time as a function of seeding phase of the bubble (with the same parameters as in Fig. 4). The circles represent experimental data; the solid line shows the numerical calculation with best fit acoustic pressure of p_a=159 kPa and proper phase calibration; the dashed lines correspond to ±4.5% deviation of laser pulse energy.

potential energy of the bubbles versus laser-pulse energy is performed. In this way, the approximate change of the maximum bubble radius with E_L can be calculated. With the compressibility taken as constant, the bubble's equilibrium radius for given E_L is obtained. We assume that small changes in the laser energy result in only a small variation of the length of the plasma channel, so that the change of the initial bubble radius can be approximated via linear breakdown theory for Gaussian pulses. Furthermore, the Rayleigh length is fitted to account for self-focusing of the laser pulse [13]. The initial velocity of the bubble is adjusted so that the new maximum radius is reached. The dashed lines in Fig. 4 show the simulation results for deviation of the laser-pulse energy of ±4.5%.

Having the bubble's initial data, simulations for a range of phase offsets φ_s at different amplitudes p_a of the sound field are performed. The acoustic pressure p_a and the phase calibration are determined by searching for the best match between the calculated collapse time versus seeding phase curve and the experimental curve (Fig. 5). The collapse time is defined here by the instant the bubble reaches its minimum radius, provided it is smaller than the initial radius $R(0)$. In this way a sound pressure amplitude of about 159 kPa is inferred.

IV. RESULTS

Figures 6–12 present the experimental data on cavitation luminescence and the dynamics of bubbles generated at different seeding phases φ_s.

The upper part of each figure shows a bar graph of the light emission. As the photon count was low, the photomultiplier signals digitized by the oscilloscope were divided into 40 bins of length 0.4 μs. In each bin the number of signal peaks exceeding a threshold value (3 mV) slightly above the noise level were counted and summed up for 100 laser shots. Thus, each bar graph presents the integrated, coarse-grained temporal distribution of cavitation luminescence at the corresponding seeding phase. For comparison, the acoustic driving signal is plotted along with the luminescence graph. In

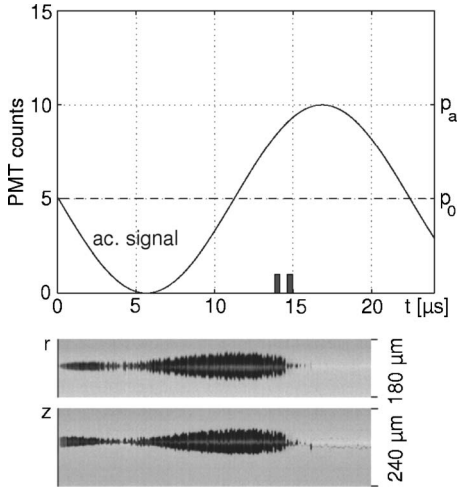

FIG. 6. Experimental data for a bubble shot at time t=0 which corresponds to a phase of the sound field φ_s=184°. Cavitation luminescence as a function of time is given in the graph at the top, together with the acoustic driving signal. At the bottom two pseudostreak images show the lateral (r) and longitudinal (z) extensions of the bubble measured immediately after the photomultiplier tube (PMT) measurements.

the bottom part of the figures two pseudostreak images of the corresponding bubble dynamics are given using the same timeline as the bar graph. These images are derived from full-frame image sequences taken immediately after the PMT measurements. Pixel rows and columns, respectively, along the maximum extension of the bubble in the direction of the laser beam axis (longitudinal size, lower trace) and perpendicular to it (lateral size, upper trace) are extracted and joined together to produce the pseudostreak images.

As in previous investigations [13] femtosecond-laser-generated bubbles without sound excitation [compare Fig. 3(a)] showed no evidence of cavitation luminescence. The current data, however, reveal that ultrasonically excited bubbles of this origin definitively emit light, albeit weak, at certain seeding phases. The light pulses coincide with the

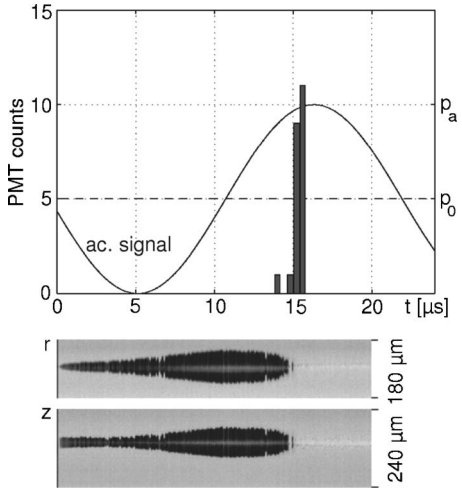

FIG. 7. Luminescence and dynamics of a bubble with seeding phase φ_s=192°.

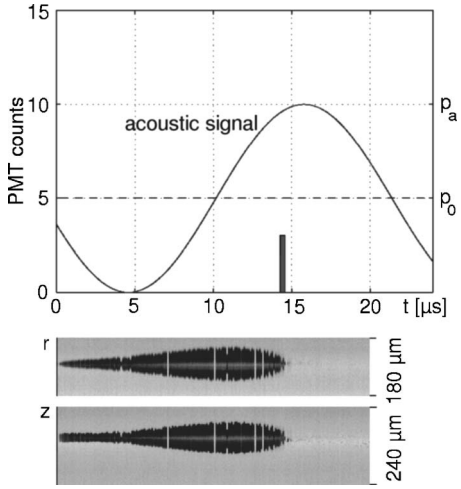

FIG. 8. Luminescence and dynamics of a bubble with seeding phase $\varphi_s=201°$.

bubble collapse within the experimental resolution, as should be expected. Small displacements between luminescence maximum and time of bubble collapse, as visible in some of the figures, are caused by gradual shifts of experimental conditions between the recording of light signals and of image sequences. The finite width of the luminescence distribution, for example seen in Fig. 7, can be explained by fluctuations of the laser-pulse energy, and thus of collapse times, during the observation time. This jitter is also present in the partly frayed appearance of the pseudostreak images. Blank columns in the streak traces are caused by bubbles of insufficient energy that collapsed shortly after breakdown and could not be expanded by the sound field.

The bubbles that emit maximum light are generated shortly after the beginning of the tension phase of the acoustic field and collapse near the maximum of the overpressure

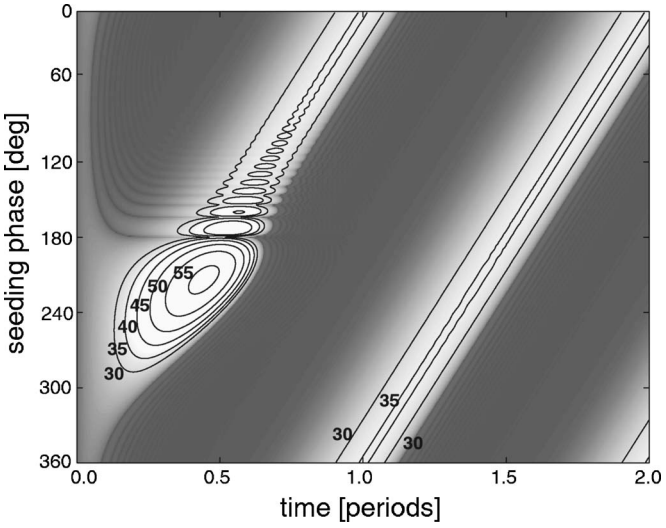

FIG. 9. Gray-scale plot of the numerically calculated radius as a function of time (horizontal axis) and seeding phase (vertical axis) for a bubble driven at $f_a=44.6$ kHz and $p_a=159$ kPa. Initial data and equilibrium radius are given in the text. The superimposed contour lines are labeled by the corresponding radius values in μm.

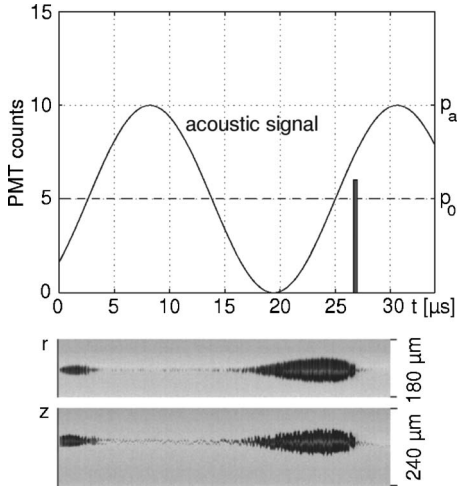

FIG. 10. Luminescence and dynamics of a bubble shot at phase $\varphi_s=323°$. Data are represented as in Fig. 6. The bubble flashes at the delayed strong collapse.

phase (Fig. 7, optimum phase $\varphi_s=192°$). Interestingly, already small changes in phase decrease luminescence yield significantly (Fig. 6, $\varphi_s=184°$, and Fig. 8, $\varphi_s=201°$). Only bubbles generated in a small window of seeding phases of about 7° width do emit detectable luminescence in the first collapse.

To check whether this effect can be attributed to changes in the bubble dynamics the numerically calculated radial dynamics as a function of phase is given in Fig. 9. The figure clearly shows that a maximum radius larger than that of the settled bubble can be achieved in a phase range between $\varphi_s\approx 190°$ and $\varphi_s\approx 260°$. The peak value of radius occurs at about 210°, which is somewhat larger than the experimentally determined phase of 192° for maximum luminescence. For phases below 192° the expansion ratio decreases. This could explain the decline of light emission in that range. For phases above 192° it appears that the strong dependence of luminescence on phase cannot be attributed to changes of bubble size or collapse speed alone.

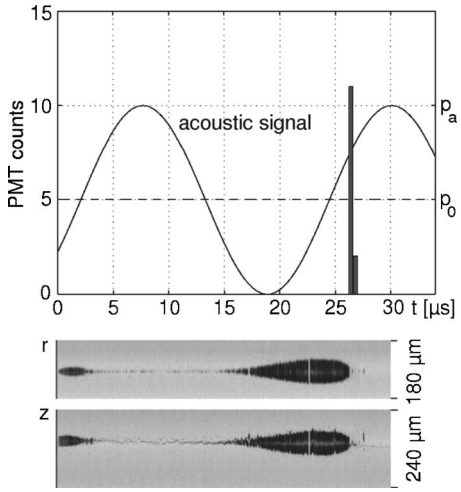

FIG. 11. Luminescence and dynamics of a bubble with seeding phase $\varphi_s=331°$.

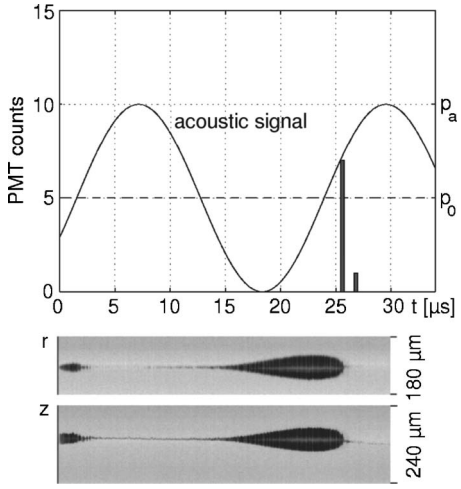

FIG. 12. Luminescence and dynamics of a bubble with seeding phase $\varphi_s = 340°$.

Even at maximum brightness the recorded luminescence corresponds to only a small number of photons per flash. Taking into account the solid angle subtended by the effective entrance area of the detection system, the quantum efficiency and gain of the photomultiplier tube, and assuming a pulse duration of ≈300 ps (width of PMT impulse response) and transmission losses of about 50%, the number of equivalent photons at $\lambda \approx 400$ nm can be roughly estimated to be of the order of a few times 10^4. This is two orders of magnitude smaller than the number of photons emitted by a typical SBSL bubble.

The light emission of bubbles generated by nanosecond laser pulses near a rigid wall depends sensitively on the standoff parameter [5]. This suggests that when the laser focus approaches the wall, the perturbation of collapse by the boundary strongly diminishes and finally prevents energy focusing and sufficient heating of the bubble medium. An analogous effect may explain the missing cavitation luminescence from the elongated nondriven bubbles generated by femtosecond laser breakdown.

Since the ultrasonically excited bubbles investigated here do not have perfect spherical symmetry [Fig. 3(b)], we have attempted to relate the bubble's eccentricity shortly before collapse to the emitted light. To this end, the ratio $\varepsilon = a/b$, where a is the lateral and b the longitudinal extension of the bubble, is determined and averaged for the last five image frames before collapse, which cover a time interval of 0.5 μs. The results of this analysis are given in Table I, part (i). Though the number of data points is limited, a correlation between sphericity (ε near 1) and recorded light energy can be stated. Note that with increasing phase the bubble shape shortly before collapse changes from a prolate form ($\varepsilon < 1$) to an oblate one ($\varepsilon > 1$).

The relation between collapse time and seeding phase (Fig. 5) shows a steep increase at $\varphi_s \approx 180°$. At this phase and beyond the action of the sound field prevents immediate collapse and the bubble is expanded to a larger size with increased collapse time. For example, the bubble of Fig. 6 is halted shortly before collapse and forced to reexpand. For bubbles created at seeding phases below 180° the first collapse occurs already after a few μs. It is followed by a series of fast afterbounces that are terminated in the tension phase of the sound field by a large radial excursion and a strong collapse. For a certain range of seeding phases, light emission from this collapse can be observed. Figures 10–12 present three examples from this range, where Fig. 11 corresponds to the case of maximum light emission. Again, this maximum is associated with best spherical symmetry of the bubble. Table I, part (ii), gives the corresponding values of ε together with the light-pulse count.

TABLE I. Number of luminescence pulses accumulated over 100 laser shots vs seeding phase φ_s and corresponding ratio ε of the semi axes of the bubbles.

	Phase (deg)	ε	Counts
(i) Immediate strong collapse	184	0.97	2
	192	1.03	22
	201	1.07	3
(ii) Delayed strong collapse	323	0.96	6
	331	0.99	13
	340	0.97	8

V. DISCUSSION

The current experiment represents an attempt to upscale bubble collapse of laser-generated bubbles. The positive results on size enlargement and light emission show that upscaling is in fact possible, though not to the degree expected beforehand. The very mechanism of their generation may prevent further upscaling of laser-induced bubbles without further measures.

We suppose that the bubble medium at collapse is composed mainly of the gas and vapor formed in the aftermath of the laser breakdown, the vapor content being changed by evaporation and condensation during the transient oscillation. Gas diffusion into the bubble is negligible on the short time scales considered [19]. Compared to stable SBSL bubbles, virtually no noble gas is present in the bubbles investigated here. Molecular gas (mainly H_2, O_2) and vapor, on the other hand, will be dissociated in the crushing bubble and yield reactive species that undergo a number of chemical reactions [20]. As, in particular, the dissociation of H_2O and O_2 is strongly endothermic, the reactions taking place in the course of the collapse of laser-induced bubbles could limit the temperature of the medium, adversely affecting cavitation luminescence. Numerical models of SBSL bubbles predict that water vapor is trapped during the fast collapse [20] and that this phenomenon may prevent the upscaling of sonoluminescence [21]. Vapor trapping certainly is effective in laser-generated bubbles as well, though a prediction of the vapor content at first collapse is more difficult, as a newly generated bubble contains a large amount of hot vapor and may not reach equilibrium conditions during the first oscillation. Our observation that the maximum of light emission versus phase φ_s does not correspond to maximum bubble

expansion may, in part, be explained by the effect of vapor trapping. At collapse the taller bubble should contain more vapor, which counteracts heating and light generation. However, we believe that the modest change of maximum bubble radius with phase around the optimum values (192°, 331°) cannot account for the immediate suppression of luminescence outside the small phase intervals reported above.

The presented correlation of light output with bubble sphericity hints at the equally important role of collapse symmetry for explaining the variation of luminescence with seeding phase. This finding is consistent with the idea that the bubble medium is not heated homogeneously upon compression and luminescence light originates from a hot-core region [22] generated by converging compression or shock waves that detach from the bubble wall in the late stages of the collapse. Shape perturbations could therefore affect the focusing of these waves and so reduce peak temperatures and pressures and light emission. This view is supported by molecular-dynamics simulations of elliptical bubbles [23].

Further simulations of the dynamics and chemistry of the bubble medium are currently performed by this method. Experiments are on their way to study the dependence of light emission on different parameters and to explore possibilities for enhancing the light output.

[1] W. Lauterborn, Acustica **31**, 51 (1974).
[2] Y. Tomita and A. Shima, Acustica **51**, 161 (1990).
[3] W. Lauterborn, T. Kurz, R. Mettin, and C. D. Ohl, in *Advanves in Chemical Physics*, edited by I. Prigogine and S. A. Rice (John Wiley & Sons, New York, 1999), Vol. 110, Chap. V, pp. 295–380.
[4] A. Philipp and W. Lauterborn, J. Fluid Mech. **361**, 75 (1998).
[5] C. D. Ohl, Phys. Fluids **14**, 2700 (2002).
[6] A. G. Akmanov, V. G. Ben'kovskii, P. I. Golubnichii, S. I. Maslennikov, and V. G. Shemanin, Sov. Phys. Acoust. **19**, 417 (1974).
[7] C. D. Ohl, O. Lindau, and W. Lauterborn, Phys. Rev. Lett. **80**, 393 (1998).
[8] O. Baghdassarian, B. Tabbert, and G. A. Williams, Phys. Rev. Lett. **83**, 2437 (1999).
[9] M. P. Brenner, S. Hilgenfeldt, and D. Lohse, Rev. Mod. Phys. **74**, 425 (2002).
[10] D. X. Hammer, E. D. Jansen, M. Frenz, G. D. Noojin, R. J. Thomas, J. Noack, A. Vogel, B. A. Rockwell, and A. J. Welch, Appl. Opt. **36**, 5630 (1997).
[11] J. Noack and A. Vogel, IEEE J. Quantum Electron. **35**, 1156 (1999).
[12] K. Tsiglifis and N. A. Pelekasis, Phys. Fluids **17**, 102101 (pages 18) (2005).
[13] R. Geisler, *Untersuchungen zur laserinduzierten Kavitation mit Nanosekunden- und Femtosekundenlasern* (Universitätsverlag Göttingen, Göttingen, 2004).
[14] T. G. Leighton, *The Acoustic Bubble* (Academic Press, London, 1994).
[15] C. D. Ohl, Phys. Rev. E **61**, 1497 (2000).
[16] B. Wolfrum, T. Kurz, O. Lindau, and W. Lauterborn, Phys. Rev. E **64**, 046306 (2001).
[17] F. R. Gilmore, Hydrodynamics Laboratory Report No. 26–4, California Institute of Technology (1952).
[18] A. Prosperetti and A. Lezzi, J. Fluid Mech. **168**, 457 (1986).
[19] I. Akhatov, O. Lindau, A. Topolnikov, R. Mettin, N. Vakhitova, and W. Lauterborn, Phys. Fluids **13**, 2805 (2001).
[20] B. D. Storey and A. J. Szeri, Proc. R. Soc. London, Ser. A **456**, 1685 (2000).
[21] R. Toegel, B. Gompf, R. Pecha, and D. Lohse, Phys. Rev. Lett. **85**, 3165 (2000).
[22] D. J. Flannigan and K. S. Suslick, Nature (London) **434**, 52 (2005).
[23] B. Metten, *Molekulardynamik-Simulationen zur Sonolumineszenz* (Der Andere Verlag, Osnabrück, 2001).